Effects of quantum interference in multiwaveguide systems bridged by Jaynes-Cummings emitters

Zhen-Rui Li,[1] Junhua Dong,[1] Yafang Xu,[2] Bingsuo Zou,[3] and Yongyou Zhang[1,*]

[1]*Key Lab of Advanced Optoelectronic Quantum Architecture and Measurement (MOE), School of Physics, Beijing Institute of Technology, Beijing 100081, China*

[2]*College of Physics Science and Technology, Yangzhou University, Yangzhou 225002, China*

[3]*MOE and Guangxi Key Laboratory of Processing for Non-ferrous Metals and Featured Materials, School of Physical Science and Technology, Guangxi University, Nanning 530004, China*

(Received 16 November 2021; revised 30 April 2022; accepted 9 May 2022; published 19 May 2022)

Quantum interference, responsible for a number of resonant optical phenomena, always intrigues researchers because of its application in optical devices. This work studies it in multiwaveguide systems bridged by Jaynes-Cummings emitters (JCEs) based on the scattering matrix theory. Two types of quantum interference are distinguished here. The first is between the incident wave and those scattered from the JCEs, while the second is only among those scattered waves. The first type leads to the two transmission valleys at the two eigenfrequencies of the JCEs in single-waveguide–single-JCE coupled systems. However, the second type is responsible for the narrow transmission peaks in single-waveguide–multi-JCE coupled systems, locating in the above transmission valleys. This work first shows the properties of the second type of quantum interference in detail and then discusses its two applications. On the one hand, the second type of quantum interference can be used to tailor the transmission spectra to achieve the electromagnetically-induced-transparency-like line shapes with a large group delay. On the other hand, it can also lead to the single-photon jumping between two certain waveguides with a nearly 100% chance in multiwaveguide systems by switching on or off some of the couplings of the JCEs to the waveguides. These applications with small peak widths commonly require a small loss and might have potential in quantum informatics.

DOI: 10.1103/PhysRevA.105.053712

I. INTRODUCTION

In the past few decades, the transport properties of single photons (SPs) in optical waveguides (WGs) [1–5] have attracted extensive interest due to the related potential applications in quantum technologies, optical quantum computation, and so on [6–16]. Platforms of optical quantum WGs include optical nanofibers [9,17,18], superconducting microwave transmission lines [6,19,20], and diamond WGs [21,22]. Since the SPs in these WGs hardly interact with the environment, they are often taken to be ideal carriers of quantum information. To control the flight of SPs, quantum emitters, such as optical cavities [2,5], two-level atoms [12,23–30], quantum dots [31–33], Jaynes-Cummings emitters (JCEs) [34–36], and superconducting qubits [37], are commonly used. These quantum emitters scatter the incident SPs backward or forward. In single-WG systems, the quantum interference between the incident wave and the scattered ones can lead to the transmission valleys [23,38], with zero transmissivity at the eigenfrequencies of quantum emitters, which has potential in designing SP switches [14,39,40], SP routers [36,39,41–47], electromagnetically induced transparency (EIT) [48–50], Fano resonance [51–53], atomic mirrors and cavities [54–57], and so on. In the case with multiple quantum emitters, the quantum interference among the scattered waves from multiple quantum emitters would unavoidably occur, and its physical origination distinguishes it from that between the incident wave and the scattered ones. Accordingly, these two types of quantum interference will generate different phenomena for the SP transport in WGs. To distinguish them, we call the quantum interference between the scattered waves due to quantum emitters and the incident one the first type and that only among the scattered waves the second type throughout this work.

Quantum interference implies that all participating light fields superpose to form a resultant field with greater, lower, or similar amplitude. Constructive and destructive interferences stem from the interaction of fields that have identical (or nearly identical) frequencies. Quantum interference affects the transport properties of the SPs to a large extent. As mentioned above, the first type of quantum interference is responsible for the transmission valleys at the eigenfrequencies of quantum emitters [23,38]. However, the second type can further produce the narrow transmission peaks in the transmission valleys [5,26]. Hereafter, the transmission valleys always represent those due to the first type of quantum interference, while the narrow transmission peaks correspond to those due to the second type of quantum interference for clarity. Generally speaking, the width of the transmission valleys is much larger than that of the narrow transmission peaks, which will be confirmed in the following contexts.

*Author to whom correspondence should be addressed. yyzhang@bit.edu.cn

Researchers did not distinguish the second type of quantum interference from the first type previously. This work will mainly focus on the second type of quantum interference and its influence on the SP transport in WG-JCE coupled systems, including the single- and multi-WG cases. The JCE consists of a cavity and an embedded two-level atom [58–60]. This WG-JCE coupled system is more general than the structure with a single WG coupled to a chain of two-level atoms [26]. Therefore, more potential applications can be expected, two of which are discussed in this work. The first one is that the second type of quantum interference can be used to tailor the transmission line shape to achieve the EIT-like peaks with a large group delay. The second one is that the second type of quantum interference can induce an ∼100% chance for SP jumping between two particular WGs.

To describe the present WG-JCE coupled system, we organize this work as follows. First, we extend the scattering matrix theory previously reported [2,5,26] to suit the multi-WG systems in Sec. II. In Sec. III, the structure of a single WG coupled to several JCEs is taken as an example to show the key characteristics of the second type of quantum interference. In Sec. IV, we focus on the tailoring effect of the second type of quantum interference on SP transmission in the single-WG system and subsequently discuss a scheme for generating an ultranarrow EIT-like transmission with a large group delay. Section V shows how the second type of quantum interference induces an ∼100% chance for a SP to jump between two particular WGs, based on which a SP router is suggested. In Sec. VI, the effect of losses in the system is discussed. Finally, we arrive at a conclusion in Sec. VII.

II. MODEL AND SCATTERING MATRIX

The model consists of M identical WGs, which are bridged by N identical JCEs. One example is depicted in Fig. 1(a) with four WGs bridged by three JCEs. Obviously, it is more general than structures with no more than two WGs [26,36]. The terminals of the WGs on the left (right) are denoted as the input (output) ports, i.e., In-m (Out-m), with $m = 1, 2, \ldots, M$, and the JCEs are numbered from left to right, denoted by JCE-n, with $n = 1, 2, \ldots, N$. For clarity, the two WGs bridged by JCE-n are denoted as WG-m_n and WG-m_n+1. The Hamiltonian for such a model reads

$$H = H_{\mathrm{WG}} + H_{\mathrm{JCE}} + H_{\mathrm{I}}, \tag{1}$$

where H_{WG}, H_{JCE}, and H_{I} describe the WGs, the JCEs, and their interactions, respectively. The Hamiltonian of the WG part has the form [5,35,45,61–63]

$$H_{\mathrm{WG}} = \sum_{m=1}^{M} \int dx [\hat{L}_m^\dagger(x)\hat{\omega}(+i\partial_x)\hat{L}_m(x) + \hat{R}_m^\dagger(x)\hat{\omega}(-i\partial_x)\hat{R}_m(x)], \tag{2}$$

where $\hat{L}_m(x)$ and $\hat{R}_m(x)$ [$\hat{L}_m^\dagger(x)$ and $\hat{R}_m^\dagger(x)$] are the annihilation (creation) field operators of the leftward- and rightward-moving photons at coordinate x in WG-m. Since all WGs are taken to be identical, their energy operators are identical too, denoted as $\hat{\omega}(\pm i\partial_x)$ for the leftward- and rightward-moving photons, respectively. We linearize $\hat{\omega}(\pm i\partial_x)$ at the wave vector $\mp k_0$, that is, $\omega(\mp k) = \omega_0 - v_g k_0 \mp i v_g \frac{\partial}{\partial x}$, with k being the wave vector, v_g being the photon group velocity, and ω_0 being the intercept energy [2]. For ease of writing, the Plank constant is set to $\hbar = 1$ throughout this work.

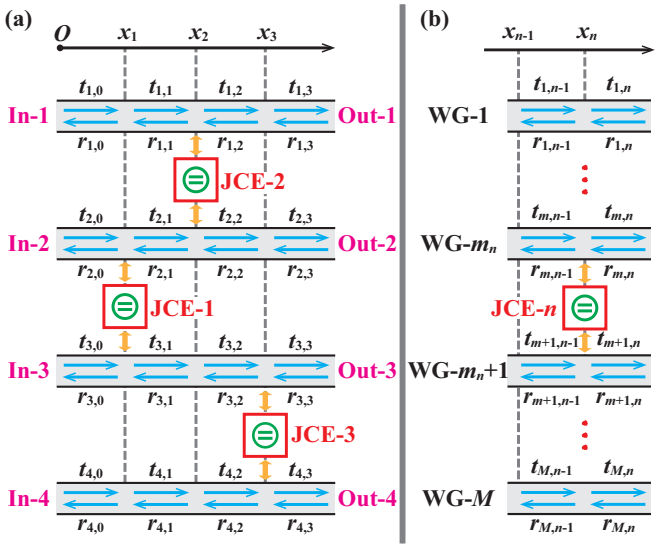

FIG. 1. (a) An example of a multi-WG model: four WGs with four input terminals (In-m, $m = 1, 2, 3, 4$) and four output terminals (Out-m) bridged by three JCEs (JCE-n located at x_n, $n = 1, 2, 3$). The JCEs are numbered from left to right. $t_{m,n}$ ($r_{m,n}$) represents the amplitude of the rightward-moving (leftward-moving) SP wave function in WG-m between positions x_n and x_{n+1}. (b) Slice of the M-WG system near JCE-n that bridges WG-m_n and WG-m_n+1. The amplitudes of the SP wave function on the left (right) side of JCE-n are denoted by $t_{m,n-1}$ and $r_{m,n-1}$ ($t_{m,n}$ and $r_{m,n}$), with $m = 1, 2, \cdots, M$. The coordinate axis Ox is given above each panel.

The Hamiltonian for the N JCEs reads [61,64,65]

$$H_{\mathrm{JCE}} = \sum_{n=1}^{N} [\omega_c \hat{c}_n^\dagger \hat{c}_n + \omega_e \hat{e}_n^\dagger \hat{e}_n + \omega_g \hat{g}_n^\dagger \hat{g}_n + \Omega(\hat{c}_n^\dagger \hat{\sigma}_n^- + \hat{\sigma}_n^+ \hat{c}_n)], \tag{3}$$

where $\hat{c}_n^\dagger$ ($\hat{c}_n$) is the bosonic creation (annihilation) operator of the cavity in JCE-n, with ω_c being the eigenfrequency. $\hat{e}_n^\dagger$ and $\hat{g}_n^\dagger$ ($\hat{e}_n$ and $\hat{g}_n$) are the electron creation (annihilation) operators in the excited and ground states with energies of ω_e and ω_g for the two-level atom in JCE-n. The atomic raising (lowering) ladder operator is defined as $\hat{\sigma}_n^+ \equiv \hat{e}_n^\dagger \hat{g}_n$ ($\hat{\sigma}_n^- \equiv \hat{g}_n^\dagger \hat{e}_n$). The cavity-atom Rabi couplings in all JCEs are denoted as Ω. Note that there are N JCEs considered in the system.

The interaction between the WGs and JCEs is described by [36,65]

$$H_{\mathrm{I}} = \sum_{n=1}^{N} \int dx V_0 \delta(x - x_n) \hat{c}_n^\dagger [\hat{L}_{m_n}(x) + \hat{R}_{m_n}(x) + \hat{L}_{m_n+1}(x) + \hat{R}_{m_n+1}(x)] + \mathrm{H.c.} \tag{4}$$

Here, the δ-type function $V_0\delta(x - x_n)$ is utilized to describe the coupling between the nth cavity and the corresponding WG-m_n and WG-m_n+1. It is suitable because the cavity width is less than the wavelength of the WG photons [66].

The single-particle eigenstate of H takes the following form [2,65]:

$$|\Phi\rangle = \sum_{m=1}^{M}\int dx[\mathcal{R}_m(x)\hat{R}_m^\dagger(x) + \mathcal{L}_m(x)\hat{L}_m^\dagger(x)]|\varnothing\rangle + \sum_{n=1}^{N}(C_n\hat{c}_n^\dagger + \mathcal{A}_n\hat{\sigma}_n^+)|\varnothing\rangle. \tag{5}$$

The vacuum state $|\varnothing\rangle$ implies that there is no photon in either the WGs or cavities and that all two-level atoms are in the ground state. C_n ($\mathcal{A}_n$) represents the excitation amplitude of the nth cavity (atom). The rightward- and leftward-moving SP wave functions $\mathcal{R}_m(x)$ and $\mathcal{L}_m(x)$ in WG-m read [26,36]

$$\mathcal{R}_m(x) = e^{ikx}\Big[t_{m,0}\theta(x_1-x) + t_{m,N}\theta(x-x_N) + \sum_{n=1}^{N-1} t_{m,n}\theta(x-x_n)\theta(x_{n+1}-x)\Big], \tag{6a}$$

$$\mathcal{L}_m(x) = e^{-ikx}\Big[r_{m,0}\theta(x_1-x) + \sum_{n=1}^{N-1} r_{m,n}\theta(x-x_n)\theta(x_{n+1}-x)\Big]. \tag{6b}$$

The unit step function $\theta(x)$ takes a value of 1 for $x > 0$, 0 for $x < 0$, and 1/2 for $x = 0$. $t_{m,n}$ and $r_{m,n}$ are the amplitudes of the rightward- and leftward-moving SP wave functions in WG-m between x_n and x_{n+1} [see Fig. 1(b)]. They can be found by substituting Eqs. (1) to (6) into the time-independent Schrödinger equation [2,64],

$$H|\Phi\rangle = \omega|\Phi\rangle,$$

where ω is the photon energy.

For a multi-WG model with JCEs, it is not an easy task to write down the solution explicitly, and thus, we turn to the scattering matrix method. The starting point is to find the transfer matrix $\boldsymbol{M}_n$ that connects the constructed vectors $\boldsymbol{F}_n$ and $\boldsymbol{F}_{n-1}$, namely,

$$\boldsymbol{F}_n = \boldsymbol{M}_n\boldsymbol{F}_{n-1}, \tag{7}$$

where

$$\begin{aligned}\boldsymbol{F}_n &= (\boldsymbol{t}_n, \boldsymbol{r}_n)^{\boldsymbol{T}},\\ \boldsymbol{t}_n &= (t_{1,n}, t_{2,n}, \ldots, t_{m_n,n}, t_{m_n+1,n}, \ldots, t_{M,n})^{\boldsymbol{T}},\\ \boldsymbol{r}_n &= (r_{1,n}, r_{2,n}, \ldots, r_{m_n,n}, r_{m_n+1,n}, \ldots, r_{M,n})^{\boldsymbol{T}}.\end{aligned}$$

T gives the transposition of the vector. WG-m_n and WG-m_n+1 are bridged by JCE-n. The transfer matrix $\boldsymbol{M}_n$ is $2M \times 2M$, and therefore, it can be divided into four $M \times M$ matrices,

$$\boldsymbol{M}_n = \begin{pmatrix}\boldsymbol{M}_n^{tt} & \boldsymbol{M}_n^{tr}\\ \boldsymbol{M}_n^{rt} & \boldsymbol{M}_n^{rr}\end{pmatrix}. \tag{8}$$

Note that there is no JCE except JCE-n in the range of $(x_{n-1},\ x_n]$ [see Fig. 1(b)]. Accordingly, these four $\boldsymbol{M}_n^{\alpha\beta}$ ($\alpha,\ \beta = r,\ t$) present a block-diagonal form, i.e.,

$$\boldsymbol{M}_n^{\alpha\beta} = \begin{cases}\begin{pmatrix}\boldsymbol{I}_{m_n-1} & & \\ & \boldsymbol{Y}_n^{\alpha\beta} & \\ & & \boldsymbol{I}_{M-m_n-1}\end{pmatrix} & \text{for } \alpha\beta = rr \text{ or } tt,\\ \begin{pmatrix}\boldsymbol{O}_{m_n-1} & & \\ & \boldsymbol{Y}_n^{\alpha\beta} & \\ & & \boldsymbol{O}_{M-m_n-1}\end{pmatrix} & \text{for } \alpha\beta = tr \text{ or } rt,\end{cases} \tag{9}$$

where $\boldsymbol{I}_j$ and $\boldsymbol{O}_j$ denote the $j \times j$ unitary and zero matrices, respectively. All $\boldsymbol{Y}_n^{\alpha\beta}$ are 2×2. After some algebra, four $\boldsymbol{Y}_n^{\alpha\beta}$ can be derived as

$$\begin{aligned}\boldsymbol{Y}_n^{tt} &= \begin{pmatrix}1-\frac{iV}{\xi} & -\frac{iV}{\xi}\\ -\frac{iV}{\xi} & 1-\frac{iV}{\xi}\end{pmatrix},\\ \boldsymbol{Y}_n^{tr} &= \begin{pmatrix}-\frac{iV}{\xi}e^{-i2kx_n} & -\frac{iV}{\xi}e^{-i2kx_n}\\ -\frac{iV}{\xi}e^{-i2kx_n} & -\frac{iV}{\xi}e^{-i2kx_n}\end{pmatrix},\\ \boldsymbol{Y}_n^{rr} &= \big(\boldsymbol{Y}_n^{tt}\big)^*,\quad \boldsymbol{Y}_n^{rt} = \big(\boldsymbol{Y}_n^{tr}\big)^*,\end{aligned} \tag{10}$$

with effective coupling strength $V \equiv V_0^2/v_g$, atomic transition energy $\omega_a = \omega_e - \omega_g$, and $\xi \equiv \omega - \omega_c - \frac{\Omega^2}{\omega-\omega_a}$. The asterisk (*) represents the conjugate operation. The zeroth points of $\xi \equiv \omega - \omega_c - \frac{\Omega^2}{\omega-\omega_a}$ determine the two eigenfrequencies of the JCE, i.e.,

$$\omega_\pm = \frac{1}{2}[\omega_c + \omega_a \pm \sqrt{(\omega_c-\omega_a)^2 + 4\Omega^2}]. \tag{11}$$

Using $\boldsymbol{M}_n$, one can naturally find the total transfer matrix by multiplying them all and therefore can also find the system transmissivities and reflectivities. However, all $\boldsymbol{M}_n$ tend to diverge near the JCE eigenfrequencies $\omega_\pm$, and consequently, the transfer matrix method is commonly infeasible for reliably calculating the transport properties of the system. This difficulty can be overcome by using the scattering matrix method. Following Ref. [36], we define the scattering matrix $\boldsymbol{S}_n$ as

$$\begin{pmatrix}\boldsymbol{t}_n\\ \boldsymbol{r}_0\end{pmatrix} = \boldsymbol{S}_n\begin{pmatrix}\boldsymbol{t}_0\\ \boldsymbol{r}_n\end{pmatrix} = \begin{pmatrix}\boldsymbol{S}_n^{tt} & \boldsymbol{S}_n^{tr}\\ \boldsymbol{S}_n^{rt} & \boldsymbol{S}_n^{rr}\end{pmatrix}\begin{pmatrix}\boldsymbol{t}_0\\ \boldsymbol{r}_n\end{pmatrix}. \tag{12}$$

Here, we also divide $\boldsymbol{S}_n$ into four $M \times M$ matrices $\boldsymbol{S}_n^{\alpha\beta}$, which can be found by an iteration method, that is [36],

$$\begin{aligned}\boldsymbol{S}_n^{tt} &= \big(\boldsymbol{W}_n^{tt} - \boldsymbol{S}_{n-1}^{tr}\boldsymbol{W}_n^{rt}\big)^{-1}\boldsymbol{S}_{n-1}^{tt},\\ \boldsymbol{S}_n^{tr} &= \big(\boldsymbol{W}_n^{tt} - \boldsymbol{S}_{n-1}^{tr}\boldsymbol{W}_n^{rt}\big)^{-1}\big(\boldsymbol{S}_{n-1}^{tr}\boldsymbol{W}_n^{rr} - \boldsymbol{W}_n^{tr}\big),\\ \boldsymbol{S}_n^{rt} &= \boldsymbol{S}_{n-1}^{rt} + \boldsymbol{S}_{n-1}^{rr}\boldsymbol{W}_n^{rt}\boldsymbol{S}_n^{tt},\\ \boldsymbol{S}_n^{rr} &= \boldsymbol{S}_{n-1}^{rr}\big(\boldsymbol{W}_n^{rt}\boldsymbol{S}_n^{tr} + \boldsymbol{W}_n^{rr}\big),\end{aligned} \tag{13}$$

where $\boldsymbol{W}_n$ is the inverse of $\boldsymbol{M}_n$, i.e.,

$$\boldsymbol{W}_n = \boldsymbol{M}_n^{-1} = \begin{pmatrix}\boldsymbol{W}_n^{tt} & \boldsymbol{W}_n^{tr}\\ \boldsymbol{W}_n^{rt} & \boldsymbol{W}_n^{rr}\end{pmatrix}. \tag{14}$$

Considering that there is no incidence on all the right terminals Out-m ($m = 1, 2, \ldots, M$), we can directly set $\boldsymbol{r}_N \equiv 0$. Accordingly, the transmissivities from In-m' to Out-m, $\boldsymbol{T}_{mm'}$, and the reflectivities from In-m' to In-m, $\boldsymbol{R}_{mm'}$, are equal to

$$\boldsymbol{T}_{mm'} = \big|\big(\boldsymbol{S}_n^{tt}\big)_{mm'}\big|^2,\quad \boldsymbol{R}_{mm'} = \big|\big(\boldsymbol{S}_n^{rt}\big)_{mm'}\big|^2. \tag{15}$$

For definiteness, we list the parameters kept unchanged throughout the work here. The units of the energy, time, wave vector, length, and group velocity, respectively, are ω_0, $\tau_0 \equiv 2\pi/\omega_0$, k_0, $\lambda_0 \equiv 2\pi/k_0$, and ω_0/k_0. All JCEs are identical to each other, and so are all WGs. For the JCEs, we take the cavity eigenfrequency $\omega_c = \omega_0$, the atomic transition energy $\omega_a = \omega_0$, and the Rabi coupling between the cavity and atom $\Omega = 0.02\omega_0$. In addition, we assume the group velocity of the WG photons $v_g = 0.6\omega_0/k_0$. The values of these parameters are consistent with those chosen in previous works [1,2,5,9,36,40].

III. SECOND TYPE OF QUANTUM INTERFERENCE

This section focuses on the properties of the second type of quantum interference in the single-WG system coupled to several identical JCEs. The key point is to understand the narrow peaks induced by the second type of quantum interference, that is, those peaks near the JCE eigenfrequencies ($\omega_- = 0.98\omega_0$ and $\omega_+ = 1.02\omega_0$) in Fig. 2 as two or more JCEs are considered. The distances between any two adjacent JCEs are all set to $d_n = 0.5\lambda_0$. For the case with one JCE, only two transmission valleys appear at the JCE eigenfrequencies due to the first type of quantum inference [see the black line with $N = 1$ in Fig. 2(a)]. Figures 2(a) and 2(b) show that the narrow peaks have the following main characteristics. (i) They appear in the two transmission valleys and are near the JCE eigenfrequencies $\omega_\pm$ [see Fig. 2(a)]. (ii) The narrow peaks near ω_- locate on the right side of ω_-, while those near ω_+ locate on the left side of ω_+ [see the enlarged version of Fig. 2(a) in Fig. 2(b)]. (iii) The number of narrow peaks increases with an increase in the number of JCEs, equal to $N - 1$. (iv) The widths of these peaks are much narrower with respect to the effective coupling strength V between the WG and cavities.

Although some of these characteristics were discussed in Refs. [5,26], their origins have not been stated clearly enough. Since these characteristics are strongly related to the potential applications of the second type of quantum interference, we here discuss their origins in detail. We start from the single-WG system coupled to two JCEs for simplicity. In this case, only one narrow peak appears [5] [see the red lines in Figs. 2(a) and 2(b)], which is consistent with the single-WG structure coupled to a chain of two-level atoms [26]. For this single-WG system coupled to two JCEs, the system transmissivity reads

$$T = \frac{1}{\{1 + \frac{V^2}{\xi^2}[\cos(2kd_1) - 1]\}^2 + \frac{V^2}{\xi^2}\left[2 + \frac{V}{\xi}\sin(2kd_1)\right]^2}. \quad (16)$$

To find the 100% transmission peaks, we set $T = 1$ in the above equation and obtain the condition as

$$\cos(2kd_1) = \frac{V^2 - \xi^2}{V^2 + \xi^2}, \quad \sin(2kd_1) = -\frac{2V\xi}{V^2 + \xi^2}. \quad (17)$$

On the one hand, Eq. (17) can identify the 100% transmission peak at ω_0. Because $\xi \equiv \omega - \omega_c - \frac{\Omega^2}{\omega - \omega_a} \to \pm\infty$ when $\omega \to \omega_0$, all terms containing $\frac{V}{\xi}$ in Eq. (17) are zero, implying $T = 1$. This situation can always occur, regardless of the values of the other parameters, for example, the distance d_1 between the two JCEs (denoted in the schematic at the top of Fig. 2). On the other hand, Eq. (17) can also identify the narrow peaks near $\omega_\pm$. As $\omega \to \omega_\pm$, we have $\xi \to 0$, and accordingly, $\cos(2kd_1) \to 1$, and $\sin(2kd_1) \to -\frac{2\xi}{V}$. Consequently, the phase $2kd_1$ should approximate $2q\pi$ (q is an integer), which gives $d_1 \sim 2q\pi/2k_0 \equiv q\lambda_0/2$. This is satisfied by Fig. 2, in which all $d_n = 0.5\lambda_0$. Let us focus on the energy point $\omega_- = 0.98\omega_0$. On this point, the wave vector k is a little less than k_0, leading to the phase $2kd_1$ being a little less than 2π. Subsequently, $\sin(2kd_1)$ is a small, negative quantity, requiring a small, positive ξ [see Eq. (17)]. This indicates that ω should be larger than ω_-; that is, the narrow peaks should locate on the right side of ω_-, which is consistent with the numerical results in Ref. [26]. The situation near the energy point ω_+ is the reverse of that near ω_-, and the corresponding

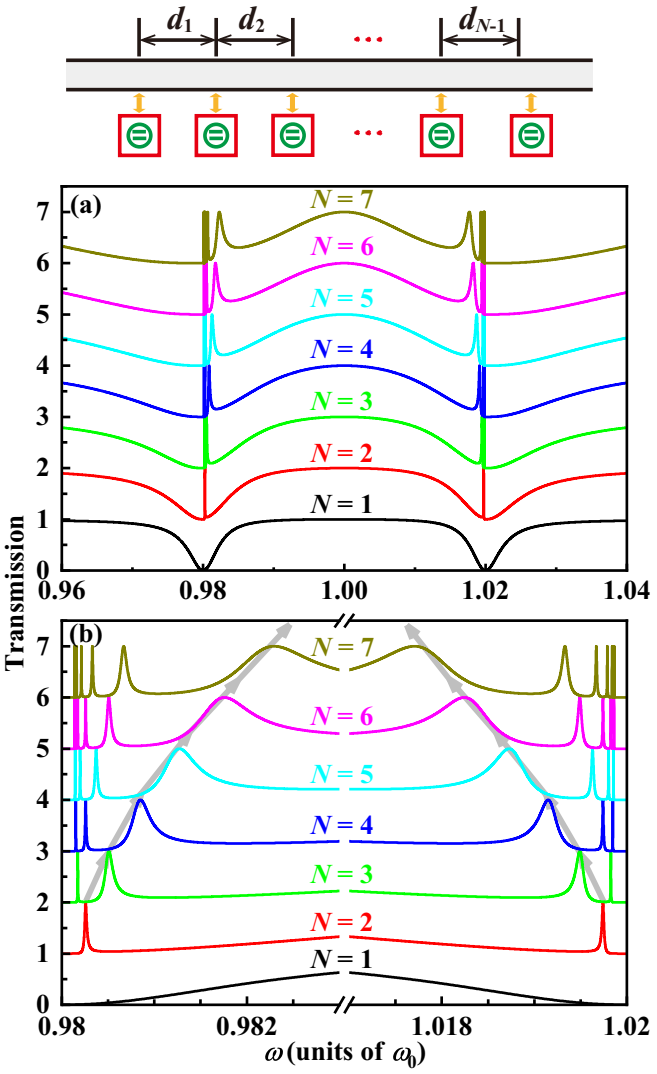

FIG. 2. (a) SP transmission spectra for a single WG coupled to a chain of N identical JCEs. (b) Enlarged version of (a) near the two eigenfrequencies of the JCEs. The schematics of the single-WG system coupled to several identical JCEs is drawn at the top. The distances between any two adjacent JCEs are set to $d_1 = d_2 = \cdots = d_{N-1} = 0.5\lambda_0$. For easy observation, the lines are offset from the bottom with a step of 1. In (a) and (b), $V = 0.005\omega_0$ is adopted.

narrow peaks locate on the left side of ω_+. Note that the first type of quantum interference between the incident wave and scattered ones from the JCEs is responsible for the wide transmission valleys, in which the narrow peaks appear due to the second type of quantum interference, which is only among the scattered waves. The forward-scattering waves from the two JCEs constructively interfere with each other. As more JCEs are introduced, it is rational to expect more narrow peaks. The conclusion is that the number of narrow peaks equals $N-1$ near each eigenfrequency of the JCE [26] (N is the number of JCEs).

The widths of the narrow peaks for the case with two JCEs [denoted as $w_\pm$ for the right and left narrow peaks; see Fig. 2(b)] can be obtained by Taylor expansion and are approximately equal to

$$\frac{w_\pm}{2V} \approx \frac{(\omega_{\rm pos}^{\pm} - \omega_\pm)^2}{V^2}, \tag{18}$$

where $\omega_{\rm pos}^{+}$ ($\omega_{\rm pos}^{-}$) denotes the position of the right (left) narrow peak. Since $\omega_{\rm pos}^{\pm}$ are very close to $\omega_\pm$, respectively, the term $|\frac{\omega_{\rm pos}^{\pm}-\omega_\pm}{V}|$ in Eq. (18) is much smaller than 1, being about 5.1%. Therefore, the widths of the narrow peaks are only about 0.26% times the widths of the transmission valleys, which are about $2V$. This narrow-width characteristic can also be observed in the case with more JCEs, for example, that with $N=7$ in Fig. 2(b). The farther the narrow peaks are away from $\omega_\pm$, the wider the narrow peaks become. For $N>3$, the complexity of the transmission formula makes it difficult to find an explicit expression for all narrow peaks. Accordingly, we will mainly study the potential applications of these narrow peaks from the numerical view. Two cases will be discussed in the following. One is transmission tailoring, which can be used to achieve an EIT-like peak with a large group delay. The other is ∼100% SP jumping between two particular WGs, which can serve as a SP router by switching on or off the couplings of the JCEs to the WGs. These two cases are given in Secs. IV and V, respectively.

IV. TRANSMISSION TAILORING

The present section focuses on the transmission tailoring of the second type of quantum interference. Since the distance between adjacent JCEs d is a crucial parameter, we plot its influence on the transmission spectra in Fig. 3(a). This influence was reported in several previous works [5,26,27,67], but their key points were not the tailoring effect discussed here.

The spectra in Fig. 3(a) correspond to the structure of a single WG coupled to two JCEs, the distance between which is denoted as d_1. Two characteristics can be identified when d_1 is away from $0.5\lambda_0$. One is that the narrow peaks gradually transform into the asymmetric Fano line shape, and the other is that the peak width becomes wider and wider. These two characteristics can be understood from Eqs. (16) to (18). The larger the value of $|\sin(2kd_1)|$ is, the larger the value of $|\omega_{\rm pos}^{\pm}-\omega_\pm|$ [see Eq. (18)] is, and therefore, the widths of the narrow peaks increase. As the Fano peaks reach the edges of the transmission valleys, they can tailor the steepness of the valley edge. In the cases with $d_1 = 0.3\lambda_0$ and $0.4\lambda_0$, the Fano peaks make the right edges steeper, while in the cases

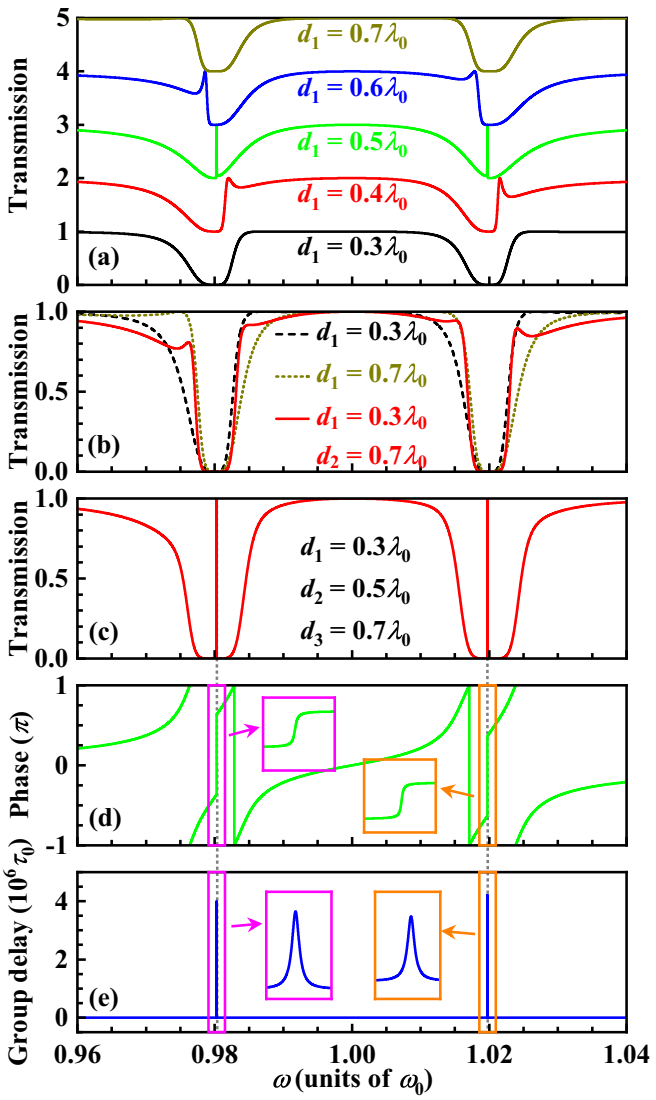

FIG. 3. (a) Transmission spectra of a single WG coupled to two JCEs with different d. Lines are offset from the bottom with a step of 1. (b) Transmission spectra of a single WG coupled to three JCEs (red solid line). For comparison, the bottom and top lines in (a) are copied as the dashed black and dotted dark yellow lines, respectively. The steepness of the transmission valleys is tailored. (c) Transmission spectra of a single WG coupled to four JCEs. (d) Phase of the transmission coefficient corresponding to (c). The two insets plot the phase variations around the two narrow transmission peaks in (c). (e) Photon group delay corresponding to (c) or (d). In all panels, $V = 0.005\omega_0$ is adopted, and the model structures are similar to that in Fig. 2.

with $d_1 = 0.6\lambda_0$ and $0.7\lambda_0$, the Fano peaks make the left ones steeper. As a rational conjecture, can the Fano peaks make both edges steeper? The answer is yes. The red solid line in Fig. 3(b) provides an example in which three JCEs are considered. The distance between the first two JCEs is set to $d_1 = 0.3\lambda_0$ and that between the last two is set to $d_2 = 0.7\lambda_0$. The right and left valley edges should coincide with the corresponding two-cavity cases with $d_1 = 0.3\lambda_0$ and $0.7\lambda_0$, respectively. For comparison, we copy the bottom and top lines in Fig. 3(a) as the black dashed and dark yellow dotted

lines in Fig. 3(b), respectively. Obviously, their corresponding edges are consistent with those of the red solid line. This tailoring effect from adjusting the distances between adjacent JCEs leads to an approximate rectangular stop band for the transmission.

Such a stop band not only displays an application as a filter intuitively but also can be used to induce the ultranarrow transmission peak. In order to demonstrate this, the four JCEs are introduced to couple to a single WG, for which the distances between adjacent JCEs are set to $d_1 = 0.3\lambda_0$, $d_2 = 0.5\lambda_0$, and $d_3 = 0.7\lambda_0$ [see Fig. 3(c)]. On the one hand, the stop bands are still retained. On the other hand, the left and right narrow peaks appear near $\omega_\pm$. These two peaks have a very small width, for which the ratio $\frac{w_\pm}{2V}$ is $\sim 7.9 \times 10^{-6}$. With respect to the ratio value of 0.26% for the two-cavity case [red solid line in Fig. 2(a)], such an arrangement of the four JCEs reduces the widths of the narrow peaks by ~300 times. When comparing this result with the narrowest peak in the case with four JCEs shown in Fig. 2 (blue line with $N = 4$), one can also find the peak width decreases ~17 times. The more valuable point may be the existence of only one narrow peak in each transmission valley, that is, a lack of perturbation from other narrow peaks.

Owing to the very small widths, the two narrow peaks in Fig. 3(c) have a wonderful property for achieving a large group delay. The phase of the transmission coefficient is plotted as a function of the photon frequency in Fig. 3(d), rapidly increasing around the two narrow peaks. For clarity, the phase variations around the two narrow peaks are enlarged; see the insets in Fig. 3(d). The first derivative of the phase with respect to the photon energy gives the group delay, which is shown in Fig. 3(e). As expected, two sharp peaks are observed, with the values being about $4 \times 10^6 \tau_0$ ($\tau_0 \equiv 2\pi/\omega_0$). This indicates that such a narrow transmission peak due to the second type of quantum interference has a potential application in photon storage [64].

To decrease the disturbance of other states on the narrow peaks, one can increase the effective coupling strength V between the WG and cavities to enlarge the width of the transmission valley [see Fig. 4(a), where the black dashed line is copied from Fig. 3(c) for comparison]. This is because the width of the transmission valley is almost proportional to V. When five JCEs are suitably arranged along the WG, two narrow peaks can be expected in each transmission valley [see Fig. 4(b), whose model structure is similar to that at the top of Fig. 2]. The four distances between two adjacent JCEs are set to $d_1 = 0.3\lambda_0$, $d_2 = d_3 = 0.5\lambda_0$, and $d_4 = 0.7\lambda_0$. In fact, if more JCEs are introduced, one can achieve more peaks in each transmission valley.

On the whole, we prove here that the transmission spectra can be tailored by using the second type of quantum interference and show the potential application of the related narrow peaks on achieving a large group delay.

V. SP JUMPING WITH ~100% CHANCE

This section focuses on multi-WG systems to study the SP jumping between two particular WGs where the second type of quantum interference plays a key role. In multi-WG systems, the second type of quantum interference can lead to

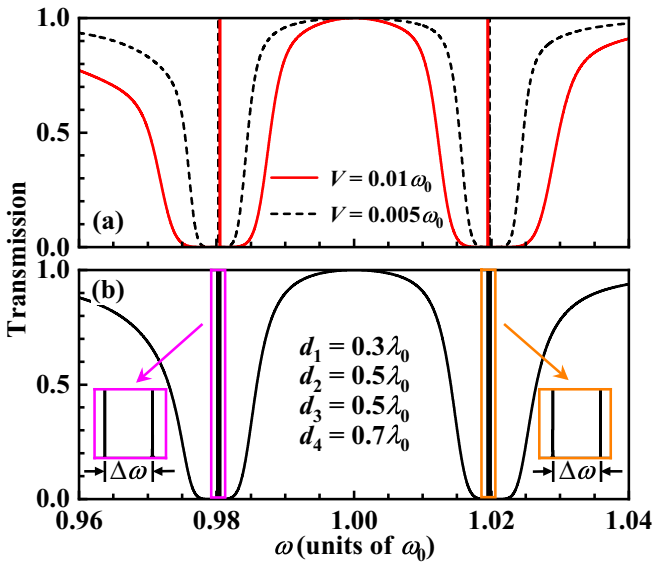

FIG. 4. (a) Transmission spectra of a single WG coupled to four JCEs with different V. The width of the transmission valley increases as V increases. (b) Transmission spectra of a single WG coupled to five JCEs. Two narrow transmission peaks can be found in each transmission valley; see the insets. In (a), we set $d_1 = 0.3\lambda_0$, $d_2 = 0.5\lambda_0$, and $d_3 = 0.7\lambda_0$, the same as the values adopted in Fig. 3(c). In (b), $V = 0.005\omega_0$ is adopted. Note that the model structures in (a) and (b) are drawn in Fig. 2.

not only the narrow transmission peaks, as discussed above, but also the narrow transmission valleys, as shown later.

The two-WG system is schematically drawn at the top of Fig. 5, where the distances between any two adjacent JCEs are all set to $d_1 = d_2 = \cdots = d_{N-1} = 0.5\lambda_0$. Since the two WGs are identical, we have $T_{11} = T_{22}$, $T_{21} = T_{12}$, and $R_{11} = R_{21} = R_{12} = R_{22}$ [see Figs. 5(a)–5(c), respectively]. Let us first focus on the case with two JCEs (i.e., $N = 2$). In this case the expressions for the transmission and reflection can be found as follows [36]:

$$\boldsymbol{T}_{11} = \boldsymbol{T}_{22} = \left| \frac{1 + i\frac{2V}{\xi} + \frac{2V^2}{\xi^2}(e^{i2kd_1} - 1)}{1 + i\frac{4V}{\xi} + \frac{4V^2}{\xi^2}(e^{i2kd_1} - 1)} \right|^2, \tag{19a}$$

$$\boldsymbol{T}_{21} = \boldsymbol{T}_{12} = \left| \frac{i\frac{2V}{\xi} + \frac{2V^2}{\xi^2}(e^{i2kd_1} - 1)}{1 + i\frac{4V}{\xi} + \frac{4V^2}{\xi^2}(e^{i2kd_1} - 1)} \right|^2, \tag{19b}$$

$$\boldsymbol{R}_{11} = \boldsymbol{R}_{22} = \boldsymbol{R}_{21} = \boldsymbol{R}_{12} = \left| \frac{\frac{2V^2}{\xi^2}(e^{i2kd_1} - 1) + i\frac{V}{\xi}(e^{i2kd_1} + 1)}{1 + i\frac{4V}{\xi} + \frac{4V^2}{\xi^2}(e^{i2kd_1} - 1)} \right|^2. \tag{19c}$$

Since $\xi = 0$ when $\omega = \omega_\pm$, all T and R are equal to $\frac{1}{4}$, indicating that the first type of quantum interference cannot induce SP jumping between the two WGs with an ~100% chance. However, T_{21} and T_{12} give narrow transmission peaks near $\omega_\pm$. Meanwhile, T_{11}, T_{22}, and all R present the narrow transmission valleys. These can be seen from the bottom black curves in Figs. 5(a)–5(c). The SP jumping between the two WGs with an ~100% chance means $T_{21} = T_{12} = 1$. Considering $\xi \approx 0$ for ω near $\omega_\pm$, we find the narrow peaks of T_{21} or

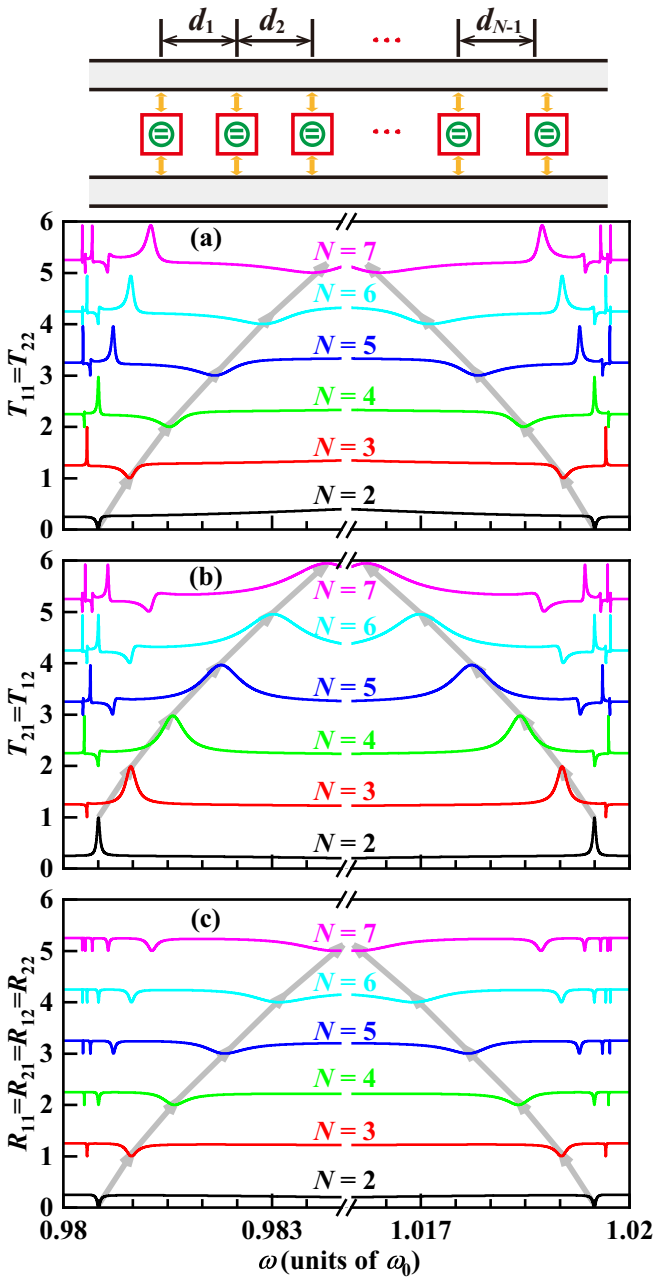

FIG. 5. Spectra (a) of $T_{11} = T_{22}$, of (b) $T_{21} = T_{12}$, and (c) of $R_{11} = R_{21} = R_{12} = R_{22}$. The schematics of the two WGs coupled to N identical JCEs is drawn at the top. The distance between any two adjacent JCEs is set to $0.5\lambda_0$, i.e. $d_1 = d_2 = \cdots = d_{N-1} = 0.5\lambda_0$. For convenience of observation, lines are offset from the bottom with a step of 1. Note that $V = 0.005\omega_0$ is adopted in all cases.

T_{12} require

$$\cos(2kd_1) \approx 1 - \frac{\xi^2}{2V^2}, \quad \sin(2kd_1) \approx -\frac{\xi}{V}. \tag{20}$$

This condition is a little different from Eq. (17), where $\cos(2kd_1) \approx 1 - \frac{2\xi^2}{V^2}$ and $\sin(2kd_1) \approx -\frac{2\xi}{V}$. Equation (20) leads to the narrow peaks and valleys all locating on the right side of ω_- and the left side of ω_+, consistent with those in single-WG systems. Under such a condition, we have $T_{21} = T_{12} \approx 1 - \frac{\xi^2}{2V^2}$. Because $|\frac{\xi}{V}| \ll 1$, the SP jumping between the two WGs can reach ~100%. Numerical calculations show that it can be up to 99.3% for the two-WG structure with two JCEs.

When more than two JCEs are introduced, the line shapes of the spectra become complicated. In the transmission spectra, not only the narrow peaks but also the narrow valleys can appear [see Figs. 5(a) and 5(b)]. There are several main characteristics, listed here for clarity. (i) The chance of the SP jumping between the two WGs (see the narrow peaks of T_{21} or T_{12} marked by the gray arrows) decreases as the number of JCEs increases. In Fig. 5(b), the chance decreases from 99.3% for $N = 2$ to 94.5% for $N = 7$ because $|\xi|$ increases as the corresponding narrow peaks gradually move away from $\omega_\pm$. This is consistent with the approximate expression $T_{21} = T_{12} \approx 1 - \frac{\xi^2}{2V^2}$ in the two-JCE case. (ii) The narrow peaks and valleys alternately appear in each transmission spectrum, consistent with the behavior of the common wave interference, i.e., alternately constructive and destructive. (iii) The total number of the narrow valleys and peaks equals $N - 1$ near each eigenfrequency of the JCE, consistent with the result in the single-WG system (see Fig. 2). (iv) The narrow peaks (valleys) of T_{21} or T_{12} correspond to the narrow valleys (peaks) of T_{11} or T_{22} [compare Fig. 5(b) with Fig. 5(a)]. (v) Only the narrow valleys exist in the reflection spectra [see Fig. 5(c)]. This is intuitive since the positions of these narrow valleys correspond to the narrow peaks of either T_{11} or T_{21} (or of either T_{12} or T_{22}).

It has been shown that the ~100% SP hopping between the two WGs can be achieved by using the transmission peaks marked by the gray arrows in Fig. 5(b). Based on this, we can further achieve the SP hopping in systems with more than two WGs by switching on or off some of the couplings of the JCEs to the WGs (see Fig. 6, where four WGs are considered as an example). Without loss of generality, the two-WG structure coupled to three JCEs, i.e., the case with $N = 3$ in Fig. 5, is used to build the model in Fig. 6. That is, any two adjacent WGs are bridged by three JCEs, which are named group 1 (G-1), group 2 (G-2), and group 3 (G-3; see Fig. 6). The distance between any two adjacent JCEs is set to $d = 0.5\lambda_0$. When the couplings of the three groups of JCEs to the WGs are all switched off, the incident SP from In-1 can be transported only to Out-1, reflected by the spectra T_{11} in Fig. 6 (the bottom black line) with a 100% chance. When the couplings of G-1 (G-1 and G-2) JCEs are switched on, the peak values of T_{21} (T_{31}) can reach 98.5% (96.7%), indicating the SP can be transported from In-1 to Out-2 (Out-3) with high efficiency. When all the couplings of the JCEs are switched on, we can get the peak values of T_{41}, which are about 94.8%. As a result, a SP router can be achieved by switching on or off the couplings of the JCEs to the WGs.

VI. EFFECTS OF LOSSES

Commonly, losses are unavoidable in experiments. This section focuses on the effects of the cavity and atom losses on the ultranarrow EIT-like transmission peak (Sec. IV) and the SP jumping between two WGs (Sec. V). Since the eigenfrequency of each cavity and their corresponding two-level atoms are tuning ($\omega_a = \omega_c$), the cavity and atom losses have almost

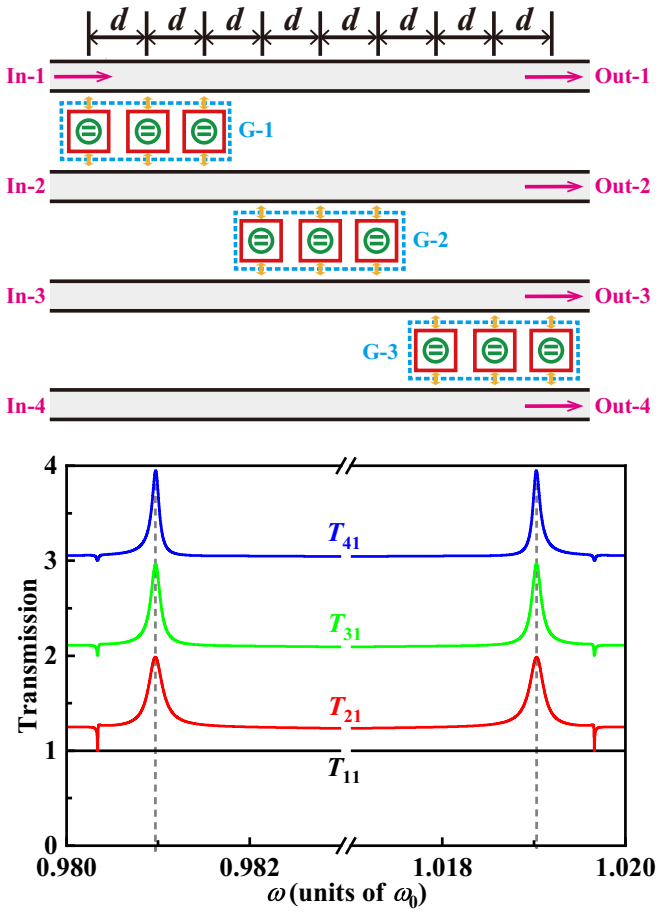

FIG. 6. Transmission spectra from In-1 to Out-m ($m = 1, 2, 3, 4$) while switching on or off some of the couplings between the WGs and JCEs. The schematics of four WGs coupled to nine JCEs is drawn at the top, and nine JCEs are separated into three groups: G-1, G-2, and G-3. The distance between any two adjacent JCEs is set to $d = 0.5\lambda_0$, and $V = 0.005\omega_0$ is always adopted. Here, the index m in T_{m1} ($m = 1, 2, 3, 4$) also means that the former $m - 1$ groups of the JCEs are switched on and the remaining groups are switched off.

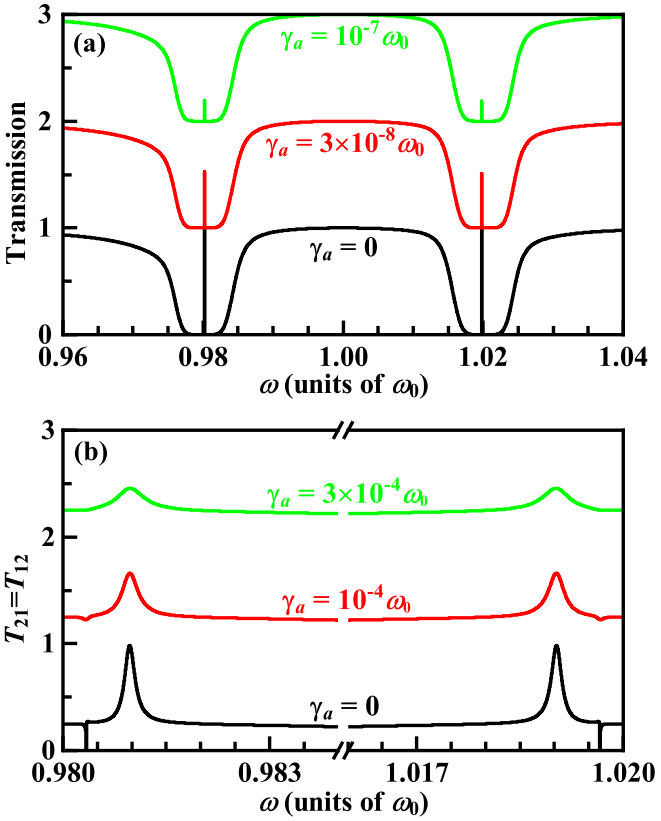

FIG. 7. (a) Transmission spectra of a single WG coupled to four JCEs with dissipative atoms. The three distances between two adjacent JCEs are set to $d_1 = 0.3\lambda_0$, $d_2 = 0.5\lambda_0$, and $d_3 = 0.7\lambda_0$, consistent with those used in Fig. 3(c). The value of the narrow peak decreases as the atom loss γ_a increases. (b) Transmission spectra of the two-WG system coupled to three JCEs with the dissipative-atom case. The structure is drawn at the top of Fig. 6, and only the couplings of the G-1 JCEs are switched on. Note that $V = 0.005\omega_0$ is adopted in all cases.

the same influence when they are less than Ω, and thus, this section takes only the effect of the atom loss as an example. The dissipation of the atom γ_a can be added by changing ω_a to $\omega_a - i\gamma_a$ in Eq. (10).

The effect of the atom losses on the EIT-like peaks in Fig. 3(c) is plotted in Fig. 7(a), where the black solid line is copied from Fig. 3(c) for comparison. In Fig. 7(a), a single WG is coupled to four JCEs with dissipative atoms. The FWHM of the black solid line in Fig. 7(a) is about $7.9 \times 10^{-8}\omega_0$. It is obvious that the value of the EIT-like narrow peaks decreases as the loss increases [see Fig. 7(a)]. When $\gamma_a = 10^{-7}\omega_0$ is larger than the FWHM, the peak value decreases to a small value. This can be understood intuitively in physics since the loss commonly corresponds to the peak width.

Such an understanding also applies to the SP jumping between two WGs [see Fig. 7(b)] since the SP jumping is also based on the narrow peaks. The model structure is drawn at the top of Fig. 6, and only the couplings of the G-1 JCEs are switched on. For comparison, we copy the red solid line in Fig. 6 as the black solid line in Fig. 7(b), whose FWHM is about $2.5 \times 10^{-4}\omega_0$. The peak value decreases with increasing γ_a. Although the peak value has an obvious decrease as $\gamma_a = 3 \times 10^{-4}\omega_0$, such a decrease is not large as $\gamma_a = 10^{-4}\omega_0$. Considering the Q factor can reach 10^4 for many types of optical cavities, the SP jumping between two WGs can be achieved in experiments. Speaking simply, the smaller the loss of the atoms and cavities in the system is, the easier achieving the narrow EIT-like shape and SP jumping between two WGs is. As a result, the narrow peaks in the transmission lines due to the second type of quantum interference commonly need a high-Q cavity.

VII. CONCLUSION

Quantum interference plays an important role in quantum phenomena and is responsible for a number of resonant phenomena in optics. This work studied two potential applications in waveguide–Jaynes-Cummings-emitter coupled systems based on existing scattering matrix theory. Two types of quantum interferences were distinguished. One is that between the incident wave and the scattered waves

from the Jaynes-Cummings emitters, and the other is that among only the scattered waves. We first derived the resonant condition of the second type of quantum interference in the case of a single waveguide coupled to two Jaynes-Cummings emitters; namely, the phase deviation between adjacent Jaynes-Cummings emitters should be $\sim 2q\pi$ (q is an integer). Then we discussed its two potential applications, i.e., single-photon transmission tailoring and single-photon jumping between two particular waveguides. The former was implemented on the single-waveguide system coupled to several Jaynes-Cummings emitters. By adjusting the distance between the Jaynes-Cummings emitters, an ultranarrow transmission peak was achieved in a transmission-stop window, which can result in an electromagnetically-induced-transparency-like transmission with a large group delay, up to 4×10^6 times the photon oscillation period. The latter application was implemented on the multiwaveguide system. The second type of quantum interference can lead to the chance of single-photon jumping between certain waveguides reaching 95%, based on which a single-photon router can be achieved by switching on or off the couplings of Jaynes-Cummings emitters to waveguides. These two applications need system losses that are approximately the same as or less than the widths of the concerned transmission peaks. They might extend the potential applications of waveguide systems in quantum informatics.

ACKNOWLEDGMENT

This work is supported by the National Natural Science Foundation of China (Grant No. 12074037).

[1] J.-T. Shen, M. L. Povinelli, S. Sandhu, and S. Fan, Phys. Rev. B **75**, 035320 (2007).
[2] J.-T. Shen and S. Fan, Phys. Rev. A **79**, 023837 (2009).
[3] J.-T. Shen and S. Fan, Phys. Rev. A **79**, 023838 (2009).
[4] S. Sandhu, M. L. Povinelli, and S. Fan, Appl. Phys. Lett. **96**, 231108 (2010).
[5] X. Zang and C. Jiang, J. Phys. B **43**, 065505 (2010).
[6] A. Wallraff, D. I. Schuster, A. Blais, L. Frunzio, R.-S. Huang, J. Majer, S. Kumar, S. M. Girvin, and R. J. Schoelkopf, Nature (London) **431**, 162 (2004).
[7] T. Yoshie, A. Scherer, J. Hendrickson, G. Khitrova, H. M. Gibbs, G. Rupper, C. Ell, O. B. Shchekin, and D. G. Deppe, Nature (London) **432**, 200 (2004).
[8] K. M. Birnbaum, A. Boca, R. Miller, A. D. Boozer, T. E. Northup, and H. J. Kimble, Nature (London) **436**, 87 (2005).
[9] B. Dayan, A. S. Parkins, T. Aoki, E. P. Ostby, K. J. Vahala, and H. J. Kimble, Science **319**, 1062 (2008).
[10] S. Hughes, Phys. Rev. Lett. **98**, 083603 (2007).
[11] L. F. Wei, Y.-X. Liu, C. P. Sun, and F. Nori, Phys. Rev. Lett. **97**, 237201 (2006).
[12] J.-T. Shen and S. Fan, Phys. Rev. Lett. **98**, 153003 (2007).
[13] J.-H. An, M. Feng, and C. H. Oh, Phys. Rev. A **79**, 032303 (2009).
[14] N.-C. Kim, J.-B. Li, Z.-J. Yang, Z.-H. Hao, and Q.-Q. Wang, Appl. Phys. Lett. **97**, 061110 (2010).
[15] L. Tan and L. Hai, J. Phys. B **45**, 035504 (2012).
[16] J. Li and R. Yu, Opt. Express **19**, 20991 (2011).
[17] C. Sayrin, C. Clausen, B. Albrecht, P. Schneeweiss, and A. Rauschenbeutel, Optica **2**, 353 (2015).
[18] S. Kato, N. Német, K. Senga, S. Mizukami, X. Huang, S. Parkins, and T. Aoki, Nat. Commun. **10**, 1160 (2019).
[19] A. F. Van Loo, A. Fedorov, K. Lalumiere, B. C. Sanders, A. Blais, and A. Wallraff, Science **342**, 1494 (2013).
[20] Y. Liu and A. A. Houck, Nat. Phys. **13**, 48 (2017).
[21] T. M. Babinec, B. J. M. Hausmann, M. Khan, Y. Zhang, J. R. Maze, P. R. Hemmer, and M. Lončar, Nat. Nanotechnol. **5**, 195 (2010).
[22] A. Sipahigil, R. E. Evans, D. D. Sukachev, M. J. Burek, J. Borregaard, M. K. Bhaskar, C. T. Nguyen, J. L. Pacheco, H. A. Atikian, C. Meuwly, R. M. Camacho, F. Jelezko, E. Bielejec, H. Park, M. Lončar, and M. D. Lukin, Science **354**, 847 (2016).
[23] J. T. Shen and S. Fan, Opt. Lett. **30**, 2001 (2005).
[24] L. Zhou, Z. R. Gong, Y.-x. Liu, C. P. Sun, and F. Nori, Phys. Rev. Lett. **101**, 100501 (2008).
[25] J. Lu, L. Zhou, H. C. Fu, and L.-M. Kuang, Phys. Rev. A **81**, 062111 (2010).
[26] T. S. Tsoi and C. K. Law, Phys. Rev. A **78**, 063832 (2008).
[27] X. F. Zang, T. Zhou, B. Cai, and Y. M. Zhu, J. Phys. B **46**, 145504 (2013).
[28] I. M. Mirza, J. G. Hoskins, and J. C. Schotland, Phys. Rev. A **96**, 053804 (2017).
[29] D. Mukhopadhyay and G. S. Agarwal, Phys. Rev. A **100**, 013812 (2019).
[30] W.-B. Yan and F.-Y. Zhang, Quantum Inf. Process. **20**, 16 (2021).
[31] D. Englund, A. Majumdar, A. Faraon, M. Toishi, N. Stoltz, P. Petroff, and J. Vučković, Phys. Rev. Lett. **104**, 073904 (2010).
[32] M.-T. Cheng and Y.-Y. Song, Opt. Lett. **37**, 978 (2012).
[33] S. Hughes, Opt. Lett. **29**, 2659 (2004).
[34] Q. Hu, B. Zou, and Y. Zhang, Phys. Rev. A **97**, 033847 (2018).
[35] Q. Jiang, Q. Hu, B. Zou, and Y. Zhang, Phys. Rev. A **98**, 023830 (2018).
[36] J. Dong, Q. Jiang, Q. Hu, B. Zou, and Y. Zhang, Phys. Rev. A **100**, 013840 (2019).
[37] S. Das, V. E. Elfving, S. Faez, and A. S. Sørensen, Phys. Rev. Lett. **118**, 140501 (2017).
[38] J.-T. Shen and S. Fan, Phys. Rev. Lett. **95**, 213001 (2005).
[39] K. Xia and J. Twamley, Phys. Rev. X **3**, 031013 (2013).
[40] C.-H. Yan and L. F. Wei, Phys. Rev. A **94**, 053816 (2016).
[41] I.-C. Hoi, C. M. Wilson, G. Johansson, T. Palomaki, B. Peropadre, and P. Delsing, Phys. Rev. Lett. **107**, 073601 (2011).
[42] L. Zhou, L.-P. Yang, Y. Li, and C. P. Sun, Phys. Rev. Lett. **111**, 103604 (2013).
[43] J. Lu, L. Zhou, L.-M. Kuang, and F. Nori, Phys. Rev. A **89**, 013805 (2014).
[44] W.-B. Yan, B. Liu, L. Zhou, and H. Fan, Europhys. Lett. **111**, 64005 (2015).
[45] X.-Y. Chen, F.-Y. Zhang, and C. Li, J. Opt. Soc. Am. B **33**, 583 (2016).

[46] W.-B. Yan and H. Fan, Sci. Rep. **4**, 4820 (2014).
[47] K. Xia, F. Jelezko, and J. Twamley, Phys. Rev. A **97**, 052315 (2018).
[48] R. D. Kekatpure, E. S. Barnard, W. Cai, and M. L. Brongersma, Phys. Rev. Lett. **104**, 243902 (2010).
[49] Y. Huang, C. Min, and G. Veronis, Appl. Phys. Lett. **99**, 143117 (2011).
[50] Z. Han and S. I. Bozhevolnyi, Opt. Express **19**, 3251 (2011).
[51] Y.-F. Xiao, M. Li, Y.-C. Liu, Y. Li, X. Sun, and Q. Gong, Phys. Rev. A **82**, 065804 (2010).
[52] X. Tu, L. Y. Mario, and T. Mei, Opt. Express **18**, 18820 (2010).
[53] H. Lu, X. Liu, D. Mao, and G. Wang, Opt. Lett. **37**, 3780 (2012).
[54] L. Zhou, H. Dong, Y.-x. Liu, C. P. Sun, and F. Nori, Phys. Rev. A **78**, 063827 (2008).
[55] D. E. Chang, L. Jiang, A. V. Gorshkov, and H. J. Kimble, New J. Phys. **14**, 063003 (2012).
[56] F. Fratini, E. Mascarenhas, L. Safari, J.-P. Poizat, D. Valente, A. Auffèves, D. Gerace, and M. F. Santos, Phys. Rev. Lett. **113**, 243601 (2014).
[57] P.-O. Guimond, A. Roulet, H. N. Le, and V. Scarani, Phys. Rev. A **93**, 023808 (2016).
[58] E. T. Jaynes and F. W. Cummings, Proc. IEEE **51**, 89 (1963).
[59] K. Fischer, S. Sun, D. Lukin, Y. Kelaita, R. Trivedi, and J. Vučković, Phys. Rev. A **98**, 021802(R) (2018).
[60] C. S. Muñoz, E. Del Valle, A. G. Tudela, K. Müller, S. Lichtmannecker, M. Kaniber, C. Tejedor, J. J. Finley, and F. P. Laussy, Nat. Photonics **8**, 550 (2014).
[61] M. Bradford and J.-T. Shen, Phys. Rev. A **87**, 063830 (2013).
[62] Y. Wang, Y. Zhang, Q. Zhang, B. Zou, and U. Schwingenschlogl, Sci. Rep. **6**, 33867 (2016).
[63] E. Rephaeli and S. Fan, Phys. Rev. Lett. **108**, 143602 (2012).
[64] G. Dong, Y. Zhang, M. A. Kamran, and B. Zou, J. Appl. Phys. **113**, 143105 (2013).
[65] C.-H. Yan and L.-F. Wei, Opt. Express **23**, 10374 (2015).
[66] Y. Zhang and B. Zou, Phys. Rev. A **89**, 063815 (2014).
[67] Z. Liao, M. Al-Amri, and M. S. Zubairy, Opt. Express **25**, 31997 (2017).